Singlet oxygen ($^1\Delta_g$)-mediated oxidation of cellular and subcellular components: ESR and AFM assays

Singlet oxygen ($^1\Delta_g$)-mediated oxidation of cellular and subcellular components: ESR and AFM assays

Bertrand Vileno[1,6]**, Małgorzata Lekka**[1,2]**, Andrzej Sienkiewicz**[1,3]**,
Pierre Marcoux**[1]**, Andrzej J Kulik**[1]**, Sandor Kasas**[4]**, Stefan Catsicas**[4]**,
Alfreda Graczyk**[5] **and László Forró**[1]

[1] Institute of Physics of Complex Matter, Ecole Polytechnique Fédérale, CH-1015 Lausanne, Switzerland
[2] The H Niewodniczański Institute of Nuclear Physics, Polish Academy of Sciences, ulica Radzikowskiego 152, 31–342 Kraków, Poland
[3] Institute of Physics, Polish Academy of Sciences, Aleja Lotników 32/46, 02-668 Warsaw, Poland
[4] Laboratoire de Neurobiologie Cellulaire, Ecole Polytechnique Fédérale, CH-1015 Lausanne, Switzerland
[5] Institute of Optoelectronics, Military University of Technology, ulica Kaliskiego 2, 00-908 Warsaw, Poland

E-mail: Bertrand.vileno@epfl.ch

Abstract

We report a comprehensive *in vitro* study of the photo-oxidative stress on different biomolecular and cellular targets generated in the presence of fullerol $C_{60}(OH)_n$, a novel, fullerene-based and water-soluble sensitizer of singlet oxygen ($^1\Delta_g$). The photodynamic efficiency of fullerol $C_{60}(OH)_n$ was checked by using a singlet oxygen scavenger, TMP-OH, and the electron spin resonance (ESR) technique, which was capable of detecting the resulting paramagnetic product, TEMPOL. ESR was also used to monitor the conformation changes occurring in the spin-labelled protein, T4L lysozyme, which was exposed to the photo-oxidative stress in solutions containing fullerol $C_{60}(OH)_n$. Finally, atomic force microscopy (AFM) experiments were performed to monitor changes in the local elastic properties of living and glutaraldehyde-fixed cells (neurons) exposed to the toxic action of $^1\Delta_g$ generated in the presence of fullerol $C_{60}(OH)_n$. Remarkably, the Young's modulus values measured for both living and fixed neurons revealed a pronounced drop as a function of exposure to the toxic action of $^1\Delta_g$. Thus, our ESR and AFM results bring evidence that the multi-hydroxylated fullerene is an efficient $^1\Delta_g$-generator in aqueous media and might be implemented as a photosensitizer for performing oxidations in biological systems.

---

[6] Author to whom any correspondence should be addressed. Fax: +41(0)21 693 4470, tel: +41(0)21 693 4304.

1. Introduction

Singlet molecular oxygen ($^1\Delta_g$) is known to be a very reactive chemical intermediate in photo-oxygenation reactions. In living cells, $^1\Delta_g$ reacts with numerous biomolecular targets such as nucleic acids, amino acids, lipids, sulfur-containing compounds, olefins, and other oxidizable species. It is believed that $^1\Delta_g$ plays a key role in photo-induced oxidative stress in humans, including UV-induced damage to the eyes and skin. On the other hand, the intentional photosensitization of singlet oxygen has found numerous applications in fields ranging from photochemistry and polymer science to biology and medicine [1]. In particular, light-induced generation of $^1\Delta_g$ has found medical applications in low-invasive and selective eradication of tumours, which is called photodynamic therapy (PDT). PDT destroys cancer cells through activation of a photosensitizer by a non-thermal laser light, which results in a direct generation of $^1\Delta_g$ at the tumour site [2].

It is now well established that biologically important heterocyclic compounds of a characteristic chemical structure that includes four pyrrole groups, like in porphyrins, reveal inherent tumour localizing properties, which is also coupled with their ability to generate reactive singlet oxygen when activated by light. Therefore, porphyrins and their derivatives are by far the most explored class of chemical compounds used in the today's PDT [3]. In fact, the porphyrin-based compound Photofrin was the first FDA approved photosensitizer for PDT human trials (1998).

Clearly, different modalities of PDT require efficient and diversified singlet oxygen photosensitizers [2], which has prompted the researchers around the globe to sensitize and characterize new compounds. Independent of the higher efficiency of light-induced cytotoxicity and the augmented degree of selectivity to different cancers, such a search for new photosensitizers will certainly broaden the scope of application of this modality.

Since their discovery in the mid-1980s [4], fullerenes have been the subject of much research as a 'third phase' of carbon for new materials science and nanotechnology. In particular, pristine fullerenes (C_{60} and C_{70}) and their derivatives generate a lot of attention due to their attractive photochemical and photophysical properties. Upon illumination with visible or UV light, both C_{60} and C_{70} reveal a high triplet quantum yield (Φ_T) that is near unity and long-lived excited triplet states [5]. The so-formed triplet states can efficiently be quenched by molecular oxygen, which results in the generation of singlet oxygen [6].

The process of singlet oxygen generation in the presence of a fullerene-based photosensitizer is schematically shown in figure 1. Illumination with light of an appropriate wavelength ($\lambda < 600$ nm) populates fullerene's short-lived singlet excited states ($^1S_n^*$). After a rapid thermalization by internal conversion (IC) to the lowest singlet excited state ($^1S_1^*$), the captured energy is then rapidly transferred *via* efficient intersystem crossing mechanism (ISC) to a long-lived excited triplet state ($^3S^*$). Subsequently, in a diffusion-controlled process, the fullerene's triplet state transfers its energy to the ground triplet state of molecular oxygen ($^3\Sigma_g^-$). The latter process, which is often referred to as a type II photoreaction mechanism, generates singlet oxygen with almost unitary yield [7].

In general, however, photosensitizers in their long-lived excited triplet states can also give rise to another mechanism of photosensitization, which involves the formation of free radicals and proceeds *via* electron or hydrogen abstraction and transfer. This alternative mechanism of photosensitization is often referred to as a type I photoreaction pathway. The type I mechanism generates reactive oxygen species, such as hydroxyl radicals ($OH^\bullet$) and superoxide anions ($O_2^{-\bullet}$), which are equally important players in photosensitized bio-oxidations as $^1\Delta_g$ [1].

Although excellent photosensitizing properties of pristine fullerenes were early and widely recognized, their applications in bio-oxidation processes have been restricted by the
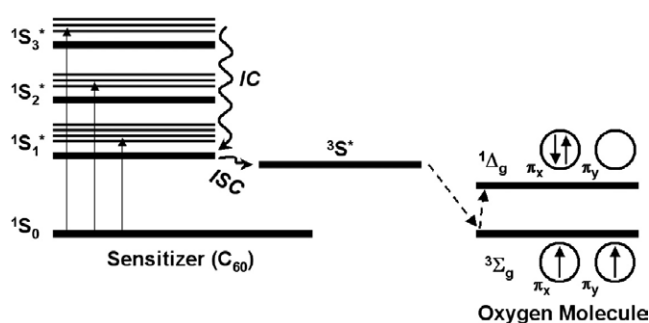
Figure 1. The Jablonski diagram showing the generation of singlet oxygen *via* a type II photoreaction mechanism. The light-induced excitation populates the short-lived singlet excited states ($^1S_n^*$) of a C_{60} molecule. This process is then followed by a rapid internal conversion (IC) to the lowest singlet excited state ($^1S_1^*$). Then, the major decay channel for the deactivation of the $^1S_1^*$ state proceeds *via* intersystem crossing (ISC), which populates the long-lived triplet state ($^3S^*$) of C_{60}. Molecular oxygen in its ground triplet ($^3\Sigma_g^-$) state effectively quenches the C_{60} triplet state ($^3S^*$), which results in the generation of singlet oxygen ($^1\Delta_g$).

lack of water-soluble derivatives. To overcome the extremely low solubility of fullerenes in aqueous solutions several strategies have been attempted, including encapsulation or microencapsulation in other carriers [8, 9], suspension obtained with the help of nonpolar co-solvents [10], and chemical functionalization (derivatization) for the introduction of hydrophilic substituents [11–13].

Among the many approaches, chemical derivatizations by the attachment of appropriate side chains have been the most widely used methodology to overcome the strong intrinsic hydrophobicity of fullerenes. Substituents ranging from water-soluble polymers, negatively charged carboxylic acids, amino acids, and hydroxyl groups to neutral polyethylene glycol have been successfully bound to C_{60} to produce its water solubility. In particular, hydroxylated C_{60} compounds, fullerols, have been found to be very soluble in physiological media [11, 14]. These novel compounds, having from 12 to 28 quasi-symmetrically attached OH groups, are now being intensively explored for their biological activity [15, 16].

In our previous study we have demonstrated that pristine fullerenes (C_{60} and C_{70}) generated singlet oxygen at high yield in organic solvents [17].

Herein, we report on the photosensitization of singlet oxygen in aqueous solutions in the presence of a novel water-soluble compound, fullerol $C_{60}(OH)_n$. First, we used electron spin resonance (ESR) to monitor $^1\Delta_g$ generation in aqueous solutions in the presence of $C_{60}(OH)_n$. Then, while also using the ESR technique, we checked the photo-oxidative potential of $C_{60}(OH)_n$ against a biomolecular target—a spin-labelled protein, lysozyme T4L. Eventually, we generated the photo-oxidative stress directly under the AFM tip in order to verify the potential of $C_{60}(OH)_n$ for performing oxidative stress at nearly physiological conditions against living and fixed cells.

2. Materials and methods

2.1. Photosensitizer

Throughout this study, a water-soluble fullerol, the multi-hydroxylated $C_{60}(OH)_n$, where n is in the range of 20–28, from Alfa Aesar Johnson Matthey GmbH, Germany, was used to generate singlet oxygen. The UV–visible absorbance spectrum of 0.1 mM aqueous solution of
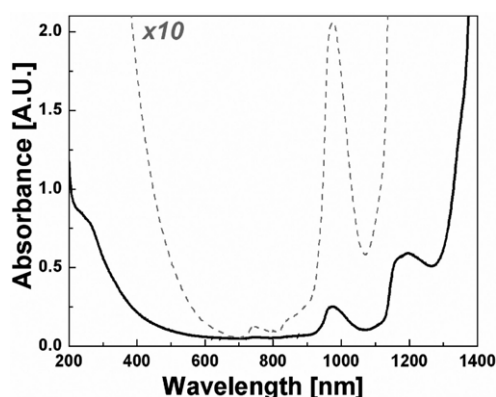
Figure 2. UV–visible absorbance spectrum of 0.1 mM aqueous solution of the commercially available fullerol $C_{60}(OH)_n$ used in this study.

fullerol $C_{60}(OH)_n$ is shown in figure 2. The spectrum indicates that fullerol $C_{60}(OH)_n$ absorbs mostly in the UV and short-wavelength regions of the visible range and, similarly to pristine C_{60}, does not exhibit strong absorption bands in the long-wavelength end of the visible range.

2.2. Electron paramagnetic resonance spectroscopy

The ESR technique provides an easy way to monitor the photosensitization of singlet oxygen in aqueous solutions. The method, which was introduced by Lion *et al* [18], is based on scavenging of singlet oxygen by a diamagnetic and water-soluble substrate molecule, TMP-OH. This process yields a paramagnetic product, the stable nitroxide radical, TEMPOL. The unpaired electron is located on the $NO^{\bullet}$ group of TEMPOL, which leads to the hyperfine splitting of the ESR signal due to interaction between the unpaired electronic spin and the nitrogen ^{14}N nucleus ($I = 1$ for ^{14}N). Therefore, the ESR signal of TEMPOL consists of three narrow hyperfine lines with a characteristic hyperfine isotropic constant A_{iso} of 17.4 G.

An ESP300E X-band spectrometer (Bruker GmbH, Biospin, Germany) equipped with a standard TE_{102} rectangular resonator was employed for acquiring the ESR spectra throughout this study. For performing measurements of the signal growth of TEMPOL as a function of illumination time, aliquots of about 7 μl of aqueous solutions containing 0.5 mM of $C_{60}(OH)_n$ and 25 mM of TMP-OH were transferred into 0.6 mm i.d. and 0.84 mm o.d. quartz capillary tubes from VitroCom, NJ, USA (sample height of 25 mm) and sealed at both ends with Cha-Seal™ tube sealing compound (Medex International, Inc., USA). The samples were exposed to the white light from a halogen source (150 W halogen lamp) using four evenly disposed glass fibre-optic light guides. Prior to the transfer into the capillaries, the samples were saturated with oxygen by bubbling oxygen through the stock solutions. The illumination of sealed aliquots was performed outside the ESR cavity at the stabilized temperature of 21 ± 1 °C.

The ESR technique also provides an approach for monitoring conformation changes of spin-labelled protein molecules. A general method for incorporating paramagnetic centres into proteins is called site-directed spin labelling (SDSL) [19, 20]. In this approach, a nitric oxide containing compound, such as the highly cysteine-specific methanethiosulfonate spin label (MTSSL), is covalently attached to a cysteine residue within the protein backbone. If a cysteine residue is not available for incorporating the MTSSL spin label, a site-directed mutagenesis is used to introduce a cysteine residue at a suitable location.

The doubly spin-labelled T4L, kindly provided by Dr H S Mchaourab (Vanderbilt University, Nashville TN, USA), was used as a molecular target for singlet oxygen in our

ESR assay of the harmful action of the photo-oxidative stress generated in the presence of $C_{60}(OH)_n$. By using the SDSL technique, the MTSSL spin labels were attached to the cysteine residues at two sites: $val^{131} \rightarrow cys$ and $thr^{151} \rightarrow cys$. Prior to measurements, the spin-labelled T4L lysozyme was mixed with $C_{60}(OH)_n$ to obtain the final concentrations 0.6 and 0.5 mM of protein and fullerol $C_{60}(OH)_n$, respectively. Afterwards, aliquots of about 7 μL of prepared solutions were transferred to into 0.6 mm i.d. and 0.84 mm o.d. quartz capillary tubes and sealed on both ends in a similar way as described above. The samples were then exposed to white light using the same experimental setup as used for the ESR monitoring of the photosensitization of singlet oxygen in the presence of $C_{60}(OH)_n$.

2.3. Atomic force microscopy

During the last few years, atomic force microscopy (AFM) has been increasingly used to investigate biological samples at molecular resolution and at nearly physiological conditions [21, 22]. Besides yielding three-dimensional topographic images of investigated objects, AFM has also become an invaluable tool for studying the important physical properties of the specimen. In particular, AFM enables one to study local mechanical properties of living cells, thus providing new insight into the structure–function relationships of such cellular components as cellular membrane and cytoskeleton. It has been demonstrated that the reorganization of cytoskeleton can be evaluated by AFM monitoring of the cellular stiffness and deformability [23]. In our recent AFM study we have shown that the oxidative damage to cells can quantitatively be described by changes in the locally measured Young's modulus [24].

The cell stiffness measurements were carried out using a commercially available AFM microscope (Park Scientific Instruments, model M5) equipped with a liquid cell. Gold-coated silicon nitride cantilevers (MLCT–AUHW, Atos GmbH, Germany) with a spring constant of 0.03 N m^{-1} were chosen for this study.

Rat primary hippocampal neurons for the AFM study were prepared according to Steiner *et al* [25]. A glass coverslip with neurons immersed in phosphate buffered saline (PBS, Sigma) was mounted into the liquid cell. Subsequently, an individual neuron was selected using an optical microscope. Initially, the AFM measurements were performed in the dark. Then, PBS buffer in the liquid cell of the AFM microscope was exchanged by a solution of fullerol $C_{60}(OH)_n$ in PBS.

The AFM measurements were performed on both living and glutaraldehyde-fixed neurons. Fixation was done using 2.5% glutaraldehyde solution in PBS buffer for 5 min. The cellular stiffness was initially measured for cells immersed in PBS and then in PBS containing 1 mM and 0.67 mM concentrations of $C_{60}(OH)_n$ for living and glutaraldehyde-fixed cells, respectively.

The force–distance curves were collected in the central part of the cell using an AFM cantilever with a pyramidal tip.

In AFM measurements, the total cantilever deflection depends on the applied force and the compliance of the investigated sample. For hard materials, such as the glass coverslip or surface of the Petri dish, the deflection directly corresponds to the sample position, which is represented by a straight-sloped force–distance plot and is usually used as a reference line that is needed for calibration. In contrast, for soft samples (like cells), the cantilever deflection is much smaller and the resulting force–distance curve has a non-linear character. The difference between these curves determines the deformation of the surface of the measured sample.

Since $^1\Delta_g$ generation was partially inhibited by antioxidants present in the culture medium, prior to the AFM measurements the cells were moved from their culture medium to PBS. After acquiring the AFM topographic image (error mode) of a chosen neuron, force-versus-distance curves were recorded around the central part of the cell in order to avoid the influence of the hard substrate (surface of the glass coverslip).
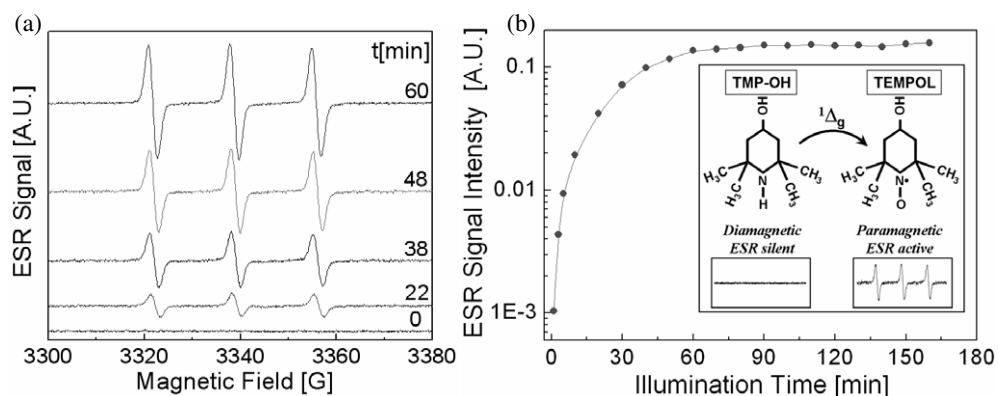
Figure 3. (a) The evolution of the ESR signal of TEMPOL as a function of illumination time in the process of photosensitization of $^1\Delta_g$ in oxygen-saturated D_2O solution containing 0.5 mM of $C_{60}(OH)_n$ and 25 mM of TMP-OH. (b) Evolution of the TEMPOL ESR signal intensity as a function of illumination time for singlet oxygen generation in 0.5 mM $C_{60}(OH)_n$ and 25 mM TMP-OH in D_2O. Inset: reactive scheme of singlet oxygen detection by ESR.

3. Results and discussion

3.1. Electron paramagnetic resonance study of $^1\Delta_g$-generation in aqueous solutions of $C_{60}(OH)_n$

The evolution of the ESR signal of the paramagnetic product, TEMPOL, resulting from the photogeneration of singlet oxygen in heavy water solution (D_2O) of $C_{60}(OH)_n$ as a function of illumination time is shown in figure 3(a).

Prior to illumination, the characteristic ESR spectrum of TEMPOL was not observed. Under illumination, the amplitude of the ESR traces of TEMPOL progressively increased for the subsequent illumination time intervals and reached saturation after about 70 min of exposure to light. A plot of the total ESR signal intensity of TEMPOL as a function of illumination time is shown in figure 3(b). The experimental points shown in this plot were determined from the double integral of the first derivative ESR spectra. The reactive scheme of detection of singlet oxygen in our ESR experiment is schematically shown in the inset to figure 3(b). Photosensitization of singlet oxygen was performed for both H_2O and D_2O solutions containing the same concentration of $C_{60}(OH)_n$. As expected for singlet oxygen-mediated processes in aqueous systems, the observed formation rates of TEMPOL were about 10 times faster for D_2O than for H_2O, which is in fairly good agreement with the isotopic enhancement of the singlet oxygen lifetime in D_2O. (The singlet oxygen lifetime of about 3 μs in H_2O increases by a factor of 10–17 in D_2O [26].)

3.2. Electron paramagnetic resonance study of singlet oxygen-mediated photo-oxidative stress on spin-labelled T4L lysozyme

Since photosensitized production of singlet oxygen is implicated in a range of detrimental oxidations of biologically important molecules, we also investigated structural damage to the spin-labelled protein molecules. Singlet oxygen-mediated photo-oxidative stress was generated in aqueous solutions containing the spin-labelled T4L lysozyme and the photosensitizer, fullerol $C_{60}(OH)_n$. The location of attachment of MTSSL spin labels to the two sites within the protein backbone of T4L lysozyme, val[131] $\rightarrow$ cys and thr[151] $\rightarrow$ cys, is shown

(a)

(b)
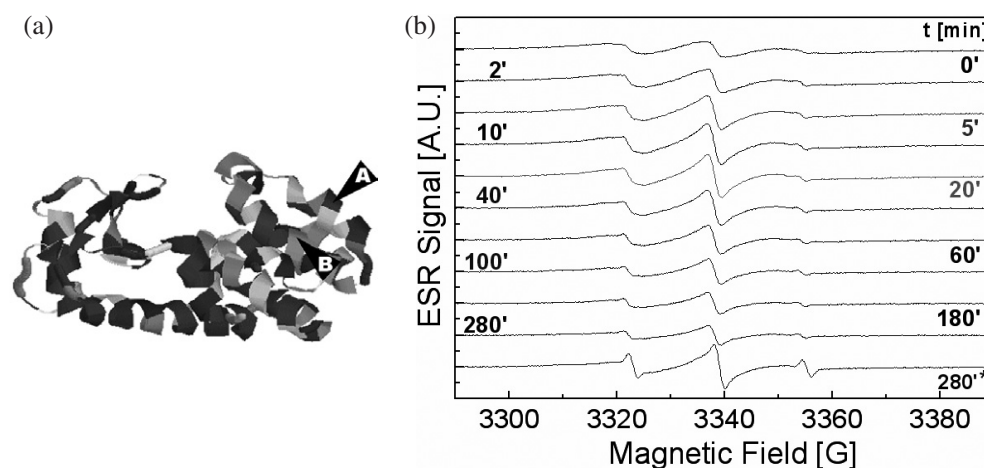
Figure 4. (a) Schematic representation of T4L lysozyme. The protein was doubly spin-labelled with the MTSSL spin label attached to the cysteine residues introduced at locations A and B, i.e. at val^{131} → cys and thr^{151} → cys, respectively. (b) Evolution of the ESR spectra of the spin-labelled protein as a function of the exposure time to the photo-oxidative stress generated in the presence of 0.5 mM concentration of $C_{60}(OH)_n$. The total illumination time is marked adjacent to each of the ESR spectra. The ESR spectrum quoted 280'* was acquired after 280 min of illumination and 48 h in the dark.

in figure 4(a). The structural alteration of protein molecules under exposure to the toxic action of singlet oxygen was followed by monitoring the evolution of the MTSSL-related ESR line as a function of illumination time. The ESR traces acquired during illumination of the aqueous sample containing 0.6 mM concentration of T4L lysozyme and 0.5 mM concentration of $C_{60}(OH)_n$ are shown in figure 4(b).

The initial trace, which was acquired prior to illumination (marked as trace 0' in figure 4(b)), reveals three broadened ESR features. The overall shape of this spectrum results from a relatively close location of the NO$^\bullet$ groups of the MTSSL spin labels residing on adjacent α-helices. Such a close distance between the spin labels leads to a very effective dipolar interaction between the neighbouring spins, which, in turn, results in a considerable broadening of the ESR features [27]. Independent of dipole–dipole broadening, the ESR spectrum of the MTSSL spin labels attached to the particular sites in a protein encodes information on the motion of the nitroxide ring. This in turn reflects the entire set of dynamic modes of the protein, including rotational diffusion of the protein, torsional oscillations about the bonds in MTSSL spin probe, local protein backbone fluctuations, and protein conformational changes. The overall evolution of the ESR traces shown in figure 4(b) reveals a progressive disappearance of the broadened components, thus pointing to protein conformational changes due to a partial denaturation of the protein. The total illumination time of T4L lysozyme sample was 280 min. It is worth noticing that in the process of photosensitization of singlet oxygen in the presence of $C_{60}(OH)_n$ we also observed a partial destruction of the MTSSL spin label.

Since the double integral of the first derivative ESR spectrum (i.e. ESR signal intensity) is directly proportional to the concentration of paramagnetic species in the measured sample, the decay of the MTSSL spin labels could be monitored quantitatively. The plot of the ESR signal intensity as a function of illumination time is shown in figure 5. As can be seen, after 280 min of exposure to the oxidative stress, the concentration of the MTSSL spin label decayed to about 20% of its initial value. The process of inactivation of spin labels occurred only during
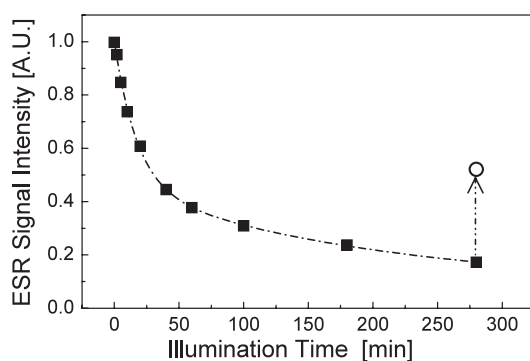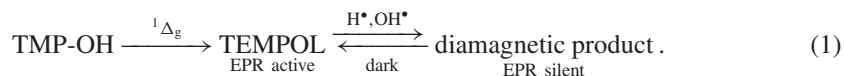
Figure 5. Evolution of the ESR signal intensity of the spin-labelled T4L lysozyme as a function of illumination time (full squares). The open circle indicates the ESR signal intensity after 280 min of illumination and 48 h spent by the sample in the dark.

illumination and was also partially reversible. Therefore, after 48 h in the dark, the MTSSL concentration recovered to about 50% of its starting level. The ESR trace acquired after 48 h of annealing in the dark is depicted in figure 4(b) (the ESR trace marked with an asterisk— 280′*), whereas the corresponding value of the partially recovered MTSSL spin concentration is indicated in figure 5 (an open circle).

The reaction of inactivation of spin labels, which accompanies the photosensitization of singlet oxygen, is mediated by free radicals (such as H$^\bullet$ and OH$^\bullet$) resulting from the type I photoreaction pathway. These processes can be summarized by the following reaction scheme (equation (1)):

$$\text{TMP-OH} \xrightarrow{^1\Delta_g} \underset{\text{EPR active}}{\text{TEMPOL}} \underset{\underset{\text{dark}}{\longleftarrow}}{\overset{\overset{\text{H}^\bullet,\text{OH}^\bullet}{\longrightarrow}}{}} \underset{\text{EPR silent}}{\text{diamagnetic product}}. \tag{1}$$

The decay of paramagnetic nitroxide radicals due to photo-oxidative processes is well documented and has been used for monitoring the oxidative strength of various systems [28]. A similar process of destruction of nitroxide spin labels was also observed by Singh *et al* in the study of the chemically generated oxidative stress on spin-labelled low-density lipoprotein (LDL) [29].

The above results demonstrate that a combination of the SDSL technique with ESR can be used to follow the conformational changes of protein molecules exposed to oxidative stress, as well as to monitor the photo-oxidative strength of the reaction milieu.

### 3.3. Atomic force microscopy assay of the oxidative stress on living and fixed neurons

Rat primary hippocampal neuronal cells were exposed to the toxic action of singlet oxygen that was photosensitized *in situ* under the AFM tip in the presence of fullerol $C_{60}(OH)_n$.

Two control assays were performed in the dark: first, cells were measured in PBS and second, AFM measurements were repeated after exchanging the regular PBS buffer by PBS containing fullerol $C_{60}(OH)_n$. Afterwards, neurons were exposed to the visible light with intervals of 10 min and directly measured after *in situ* illumination.

The experimental AFM setup used in this study is schematically shown in the left panel of figure 6. A flexible multi-core quartz light guide (4.0 mm light-guiding cross-section) delivered white light directly into the liquid cell of the AFM scanner. The right panel of figure 6 shows the scheme of AFM indentation of the investigated neurons.
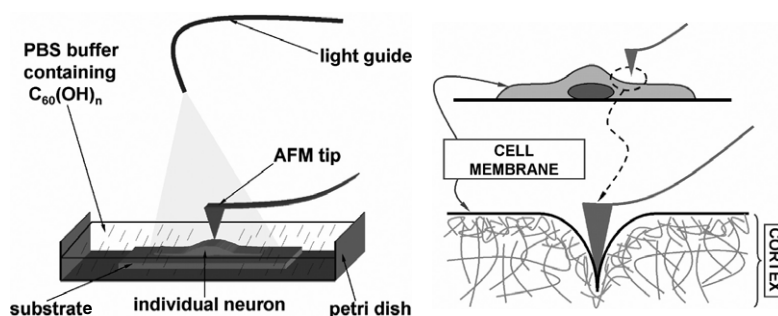
Figure 6. Schematic illustration of AFM measurements of the local elastic properties of neurons exposed to the photo-oxidative stress (left). Simplified representation of the AFM indentation of investigated neurons (right).
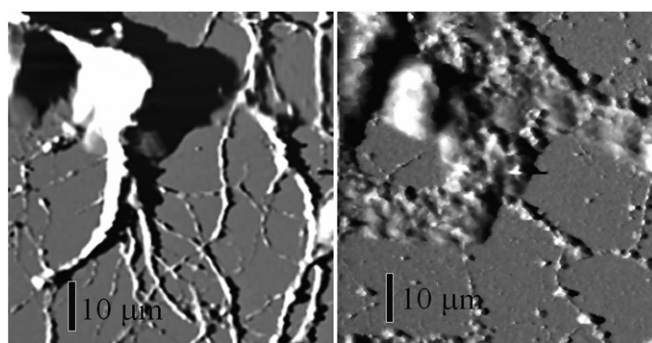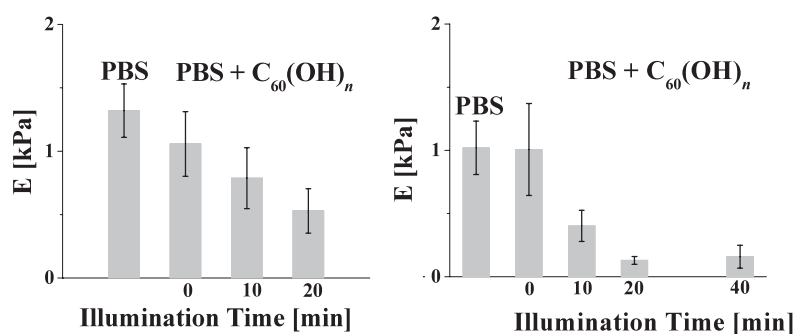

Figure 7. AFM images of the glutaraldehyde-fixed rat primary hippocampal neurons under PBS containing 0.67 mM concentration of $C_{60}(OH)_n$. The AFM images were acquired before illumination (left) and after 40 min of illumination with white light (right), respectively.

Figure 7 shows the AFM topographic images of a selected glutaraldehyde-fixed neuron measured in PBS containing 0.67 mM concentration of $C_{60}(OH)_n$ before and after the exposure to $^1\Delta_g$-mediated oxidative damage. The cellular stiffness was initially measured for cells immersed in PBS and then in PBS containing 1 and 0.67 mM concentrations of $C_{60}(OH)_n$ for living and glutaraldehyde-fixed cells, respectively. The force curves were collected in the central part of the cell. The Young's modulus values were evaluated in the frame of the *so-called* Hertz mechanics (extended later by Sneddon [30]), assuming a conical shape of the AFM tip and a flat, deformable substrate.

The calculated values for the Young's modulus for neurons are shown in figure 8. The average value and the standard deviation of the Young's modulus were determined by fitting a Gaussian distribution to the histogram of the values obtained for each curve. All the calculations were done assuming a Poisson ratio equal to 0.5 (cells were assumed to be incompressible).

As shown in figure 8, a significant decrease of the Young's modulus values as a function of illumination time was observed for both glutaraldehyde-fixed and living neurons. Although the Young's modulus values decrease somewhat more slowly for the fixed neurons (figure 8(a)) than for the living ones (figure 8(b)), this discrepancy might be accounted for by the difference of about 30% in fullerol $C_{60}(OH)_n$ concentrations used in both experiments.

It has been previously shown that AFM can detect changes occurring in the cell stiffness and cytoskeleton organization under exposure to different cytoskeletal drugs [31]. Clearly, the

Figure 8. The dependence of the Young's modulus values (E) as a function of exposure time to the toxic action of singlet oxygen for the glutaraldehyde-fixed (left) and living neurons (right).

AFM-measured changes in the local cellular stiffness (expressed in this study by the Young's modulus values) may be produced by many phenomena, including modifications occurring in the cellular membrane (like changes in the membrane permeability and continuity) and/or rearrangement of cytoskeletal filaments.

However, taking into account the actual indentation depth of 0.5 μm, the decrease of the Young's modulus values suggests that the AFM-measured local cellular stiffness most likely monitors the reorganization of the neuronal cytoskeleton at a relatively shallow depth under the cytoplasmic membrane.

Therefore, we postulate that independently of damage occurring in the cellular membrane and membrane-bound proteins, the primary oxidative processes also induce significant changes to the outer actin-rich cortex.

It is worth noticing that an additional assay of Trypan Blue staining performed for neurons exposed to 10, 20 and 50 min of $^1\Delta_g$-mediated oxidative damage revealed a significant number of dead cells only after 50 min of exposure. This result suggests that the marked AFM-detected changes in the local cellular stiffness detected already after 10 min of exposure to the oxidative stress belong rather to the primary effects induced by photo-oxidation.

Also worth noticing is the fact that a parallel comparative study of the photo-oxidative stress on living and fixed neurons performed in the presence of a well-established singlet oxygen sensitizer, the water-soluble amino acid derivative of protoporphyrin IX, PP(Ala$_2$)(Arg$_2$) [32, 33], yielded similar changes in the Young's modulus values to those observed in the presence of C$_{60}$(OH)$_n$ [34].

4. Summary

This study brings evidence that the water-soluble fullerene derivative, C$_{60}$(OH)$_n$, conserves the properties of pristine fullerenes for generating singlet oxygen *via* a type II reaction mechanism also in oxygenated aqueous solutions, and might be considered as a potent oxidizing agent in biological systems. However, it has to be stressed that although photo-catalytically active, fullerol C$_{60}$(OH)$_n$ reveals different photophysical properties than well-established protoporphyrin-based sensitizers of singlet oxygen. In particular, the strong absorption bands of C$_{60}$(OH)$_n$ do not coincide with the 'biological window' of high optical transmission of blood and tissue between 700 and 1100 nm. Notwithstanding, derivatized water-soluble fullerenes generate a lot of interest in the field of medicine for a variety of potential applications, including photodynamic therapy [35, 36]. Specifically, in contrast to the organic photosensitizers,

fullerols reveal low photobleaching and, as it was recently demonstrated by Sayes *et al*, low inherent cytotoxicity [37].

We also show that a combination of ESR and SDSL might be employed to study the conformational changes occurring in biomolecular targets, like proteins, under exposure to oxidative stress. Finally, we emphasize that AFM can be used as a sensitive tool for detecting early changes occurring in sub-cellular structures of cells that are exposed to oxidative stress. In particular, our AFM observations of the changes in the local elastic properties cells point to the actin-rich cortex and focal points as primary targets for the toxic action of singlet oxygen.

Acknowledgments

References

[1] DeRosa M C and Crutchley R J 2002 *Coord. Chem. Rev.* **233/234** 351–71
[2] Dolmans D E J G J, Fukumura D and Jain R K 2003 *Nat. Cancer Rev.* **3** 380–7
[3] Konan Y N, Gurny R and Allemann E 2002 *J. Photochem. Photobiol.* B **66** 89–106
[4] Kroto H W, Heath J R, O'Brien S C, Curl R F and Smalley R E 1985 *Nature* **318** 162
[5] Guldiand D M and Prato M 2000 *Acc. Chem. Res.* **33** 695–703
[6] Arbogast J W and Foote C S 1991 *J. Am. Chem. Soc.* **113** 8886–9
[7] Foote C S 1994 *Top. Curr. Chem.* **169** 347
[8] Mchedlov-Petrossyan N O, Klochkov V K and Andrievsky G V 1997 *J. Chem. Soc. Faraday Trans.* **93** 4343
[9] Jenekhe S A and Chen X L 1998 *Science* **279** 1903
[10] Scrivens W A, Tour J M, Creek K E and Pirisi L 1994 *J. Am. Chem. Soc.* **116** 4517
[11] Chiang L Y, Swirczewski J W, Hsu C S, Chowdhury S K, Cameron S and Creegan K 1992 *J. Chem. Soc. Chem. Commun.* **24** 1791–3
[12] Tabata Y, Murakami Y and Ikada Y 1997 *Fullerene Sci. Technol.* **5** 989
[13] An Y Z, Anderson J L and Rubin Y 1993 *J. Org. Chem.* **58** 4799
[14] Chiang L Y, Bhonsle J B, Wang L, Shu S F, Chang T M and Hwu J R 1996 *Tetrahedron* **52** 4963
[15] Wharton T, Kini V U, Mortis R A and Wilson L J 2001 *Tetrahedron Lett.* **42** 5159–62
[16] Bolskar R D, Benedetto A F, Husebo L O, Price R E, Jackson E F, Wallace S, Wilson L J and Alford J M 2003 *J. Am. Chem. Soc.* **125** 5471–8
[17] Sienkiewicz A, Garaj S, Białkowska-Jaworska E and Forró L 2000 *Electronic Properties of Novel Materials-Molecular Nanostructures (Kirchberg, Tirol, Austria, March 2000) (AIP Conf. Proc.* vol 544) ed H Kuzmany, J Fink, M Mehring and S Roth (Melville, NY: AIP) pp 63–6
[18] Lion Y, Delmelle M and Van de Vorst V 1976 *Nature* **263** 442–3
[19] Hubbell W L and Altenbach C 1994 *Curr. Opin. Struct. Biol.* **4** 566–77
[20] Hubbell W L, Gross A, Langden R and Lietzow M A 1998 *Curr. Opin. Struct. Biol.* **8** 649–56
[21] Dufrêne Y F 2002 *J. Bacteriol.* **184** 5205–13
[22] Radmacher M 1997 *IEEE Eng. Med. Biol.* **16** 47–57
[23] Lekka M, Laidler P, Ignacak J, Łabędź M, Lekki J, Struszczyk H, Stachura Z and Hrynkiewicz A Z 2001 *Biochem. Biophys. Acta* **1540** 127–36
[24] Vileno B, Sienkiewicz A, Lekka M, Kulik A J and Forró L 2004 *Carbon* **42** 1195–8
[25] Steiner P, Sarria J-C F, Glauser L, Magnin S, Catsicas S and Hirling H 2002 *J. Cell Biol.* **157** 1197–209
[26] Andersen L K and Ogilby P R 2002 *J. Phys. Chem.* A **106** 11064–9
[27] Fajer P G 2000 *Encyclopedia of Analytical Chemistry* ed R A Meyers (Chichester: Wiley) pp 5725–61

[28] Takeshita K, Saito K, Ueda J I, Anzai K and Ozawa T 2002 *Biochim. Biophys. Acta* **1573** 156–64
[29] Singh R J, Feix J B, Mchaourab H S, Hogg N and Kalyanaraman B 1995 *Arch. Biochem. Biophys.* **320** 155–61
[30] Sneddon I N 1965 *Int. J. Eng. Sci.* **3** 47–57
[31] Wu H W, Kuhn T and Moy V T 1998 *Scanning* **20** 389–97
[32] Graczyk A and Konarski J 1995 *US Patent Specification* 5,541,599
[33] Szpakowska M, Lasocki K, Grzybowski J and Graczyk A 2001 *Pharmacol. Res.* **44** 243–6
[34] Sienkiewicz A *et al* 2005 *Biophys. J.* submitted
[35] Tokuyama H, Yamago S, Nakamura E, Shiraki T and Sugira Y 1993 *J. Am. Chem. Soc.* **115** 6506
[36] Kamat J P, Devasagayam T P A, Priyadarsini K I and Mohan H 2000 *Toxicology* **155** 55–61
[37] Sayes C M, Fortner J D, Guo W, Lyon D, Boyd A M, Ausman K D, Tao Y J, Sitharaman B, Wilson L J, Hughes J B, West J L and Colvin V L 2004 *Nano Lett.* **4** 1881–7